# SPATIALLY RESOLVED SILICON SOLAR CELL CHARACTERIZATION USING INFRARED IMAGING METHODS

M. Kasemann[1,2], W. Kwapil[1], M.C. Schubert[1], H. Habenicht[1], B. Walter[1], M. The[1], S. Kontermann[1], S. Rein[1], O. Breitenstein[3], J. Bauer[3], A. Lotnyk[3], B. Michl[4], H. Nagel[4], A. Schütt[5], J. Carstensen[5], H. Föll[5], T. Trupke[6], Y. Augarten[6], H. Kampwerth[6], R.A. Bardos[7], S. Pingel[8], J. Berghold[8], W. Warta[1], S.W. Glunz[1]

[1] Fraunhofer Institute for Solar Energy Systems (ISE), Heidenhofstr. 2, 79110 Freiburg, Germany
phone: +49 761 4588 5321, e-mail: martin@kasemann.net
[2] University of Freiburg, Material Research Center, Stefan-Meier-Str. 21, 79104 Freiburg, Germany
[3] Max Planck Institute for Microstructure Physics, Weinberg 2, 06120 Halle, Germany
[4] SCHOTT Solar GmbH, Carl-Zeiss-Straße 4, 63755 Alzenau, Germany
[5] University of Kiel, Kaiserstr. 2, 24143 Kiel, Germany
[6] The University of New South Wales, Sydney, 2052, NSW, Australia
[7] BT Imaging Pty Ltd, 18 Bulletin Place, Sydney, 2000, NSW, Australia
[8] Solon AG, Am Studio 16, 12489 Berlin, Germany

## ABSTRACT

We present a comprehensive overview over infrared imaging techniques for (electrical) silicon solar cell characterization. Recent method development in local series resistance imaging is reviewed in more detail and new results in local breakdown investigations on multicrystalline (mc) silicon solar cells are reported. We observe local junction breakdown sites on industrial mc-cells at reverse voltages as low as -7V and breakdown in great areas of the cell at voltages around -14V. As these breakdown sites (as well as local shunts) can cause hot spots which can damage the cell and the module, we also present an ultra-fast, simple and quantitative method for hot-spot detection. Typical measurement times in the order of 10 milliseconds are achieved.

## INTRODUCTION AND METHOD OVERVIEW

With the development of fast and low-noise charge coupled device (CCD) detectors in different wavelength ranges, infrared imaging methods found numerous applications in spatially resolved solar cell characterization and quality control. In this paper, we give an overview over existing infrared imaging methods for the detection of different local solar cell properties. In a more detailed review, we will focus on the recent development in series resistance imaging. With experiments on junction pre-breakdown and the relation between pre-breakdown sites and material defects, we open an important field that requires further research. As the first pre-breakdown sites in our measurements on industrial cells appear as hot spots at reverse voltages as low as -7 V, we propose a method for reliable and ultra-fast hot spot detection for industrial production lines. With this method, we will demonstrate the detection of weak hot spots within a measurement time of only 10 milliseconds.

The basic setup used for infrared imaging methods is shown in Figure 1a. The solar cell is mounted on a (tem-

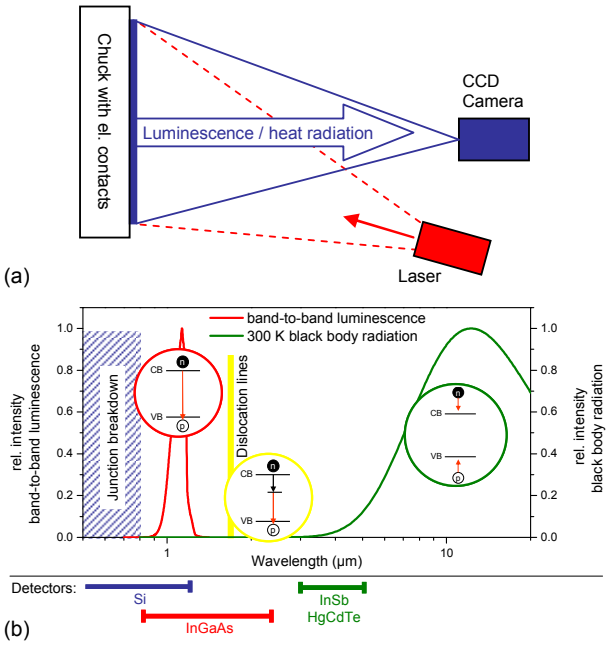


*Figure 1: (a) Infrared imaging setup. Homogeneous irradiation of the entire solar cell is typically performed with lasers in the wavelength range from 790 nm to 940 nm. Different cameras can be used to detect radiation in different wavelength ranges. (b) Spectral range of photon emission from silicon solar cells, the underlying mechanisms, and the detectors used in this contribution.*

perature controlled) measurement chuck and electrically contacted to a power supply/load. In measurement modes where illumination is required, the cell is typically irradiated with lasers in the wavelength range of 790 nm to 940 nm. Different commercially available charge coupled device (CCD) cameras can be used to image the radiation emitted by the solar cell.

The spectrum emitted by a silicon solar cell and the underlying mechanisms are given in Figure 1b. Band-to-band luminescence is emitted during a radiative recombination event of an electron and hole over the band gap. The spectrum is located around 1.1 µm. Band-to-band

| Parameter | Spectrum | Method | Short description | Ref. |
|---|---|---|---|---|
| Lifetime / Diffusion length | Thermal | CDI or ILM | Carrier Density Imaging/Infrared Lifetime Mapping on wafers. Signal ~ excess carrier density | [1,2] |
| | B2B lum. | PLI | PL imaging of wafers. Signal ~ product of electron and hole concentrations, i.e. ~ excess carrier density at low injection. | [3] |
| | B2B lum. | ELI | EL images through different filters using effects of photon reabsorption to determine carrier profile. | [4] |
| | Thermal | Voc-ILIT | ILIT Signal on cells and diffused wafers under open circuit conditions ~ to dark saturation current. | [5] |
| Interstitial iron | B2B lum. | PLI | Measure lifetime before and after dissociation of FeB at injection levels below or above the crossover point. | [6] |
| Dislocations | Defect lum. | ELI or PLI | EL or PL signal between approx. 1.2µm and 1.6µm from recombination via dislocation states in the band gap | [7] |
| Trapping | Thermal | CDI or ILM | CDI/ILM signal dominated by trapping at low injection. Quantitative determination of trap density. | [8,9] |
| Emitter sheet resistance | Thermal | SRI | Sheet resistance imaging. Thermal emission signal ~ free carrier density | [10] |
| Series resistance | B2B lum. | Rs-PLI | Different PL images. Determines Rs near MPP | [11] |
| | B2B lum. | Rs-ELI | Rs from derivative of local EL signal with respect to terminal voltage | [12] |
| | B2B lum. | RESI | Local voltage from EL, local current from DLIT and EL → Rs | [13] |
| | Thermal | Jsc-ILIT | Qualitative image affected by: 1) High signal due to heating in lateral Rs. 2) Low signal due to decreased thermalization over the junction. | [14] |
| | Thermal | Rs-DLIT | Division of two DLIT images taken at two different forward biases well above 0.5V | [15] |
| | Thermal | Rs-ILIT | Combination of MPP and Jsc image. Rs appearance affected by same processes as Jsc-ILIT. | [15] |
| Shunts | Thermal | ILIT or DLIT | Signal near ~0.5V or MPP dominated by heat dissipation in shunt. Different quantification methods. | [16] |
| | B2B lum. | PLI or ELI | Low intensity around shunt due to reduction of local junction voltage, caused by voltage drops over series resistances surrounding the shunt. | [17] |
| Junction breakdown | Thermal | TC-DLIT | Local temperature coefficient of breakdown current | [18] |
| | Thermal | MF-ILIT | Local current multiplication factor | [18] |
| | Thermal | Slope-DLIT | "Hardness" of breakdown | [18] |
| | Visible + NIR | | Small light spots in breakdown regions attributed to microplasma radiation and possible other effects. | here |
| Hot spots | Thermal | DLIT | DLIT at reverse voltage (e.g. -10V). Measures heat dissipation in relevant hot spots in 10 milliseconds. | here |
| Local efficiency | Thermal | MPP-ILIT | Signal ~ total power loss. | [5] |
| | Thermal | ILIT | Jsc-ILIT image minus MPP-ILIT image divided by Jsc-ILIT image gives local solar cell efficiency if not dominated by Rs. | [19] |

*Table 1: List of imaging methods for the measurement of different silicon solar cell parameters. Typical abbreviations are: ELI=electroluminescence imaging; PLI=photoluminescence imaging; DLIT=dark lock-in thermography; ILIT=illuminated lock-in thermography; MPP=maximum power point; Jsc=short-circuit operating point; Rs=series resistance; NIR = near infrared; B2B=band-to-band; RESI=recombination current and series resistance imaging; Voc=open circuit operating point*

luminescence can be detected with silicon sensors and with InGaAs sensors. Light emission has also been observed in a band from approximately 1.2µm to 1.6µm. It is generated by radiative recombination via different defect levels attributed to crystal defects/dislocations. [7,20-22] The "defect" lines can be detected with an InGaAs sensor combined with properly designed band pass filters. The methods based on lock-in thermography (LIT) detect the heat radiation emitted by the solar cell close to room temperature. Typical sensors materials for the detection of heat radiation are InSb and HgCdTe. Another emission spectrum of silicon solar cells is caused by junction breakdown. According to investigations compiled by Akil et al. [23,24], junction breakdown emission is found at wavelengths below approximately 880 nm through the visible range.

Many different IR imaging methods for the spatially resolved detection of different electrical properties have already been proposed. These methods are based on different detection principles, work in different production states and in different operating modes of the solar cell. A comprehensive list of accessible parameters and existing methods is given in Table 1 with references to more detailed papers.

## SERIES RESISTANCE IMAGING

The series resistance is an important parameter for the optimization of solar cell efficiencies since it has a strong influence on the fill factor. There has already been a lot of work on the determination of the global series resistance of a solar cell. Recently, five different methods for the determination of the global series resistance have been reviewed and tested for reliability. [25] But however accurate the global series resistance is measured, it allows only limited conclusions about possible *causes* for increased series resistances. Therefore, we will review different methods for the determination of a *local* series resistance that have been proposed only recently. [11-13]

The qualitative appearance of luminescence images already indicates that lateral series resistances significantly influence the luminescence signal distribution across the solar cell. Moreover, it was shown recently that even the appearance of shunts in luminescence images is governed by the effective series resistance surrounding the shunt. [17] As the luminescence signal is exponentially related to the local junction voltage, even very small voltage variations due to series resistance losses can be resolved. Consequently, several different methods for imaging the local series resistance have been proposed. Trupke et al. [11] have proposed a method called Rs-PL which measures the local series resistance based on several PL images under different conditions. Ramspeck et al. [13] have proposed a method called RESI which obtains the lateral voltage distribution on the cell from an EL image while obtaining the local current from a combination of a DLIT image and an EL image. Hinken et al. [26] have proposed a method based on several EL images using an intelligent derivative-method originally proposed by Werner et al. for current-voltage curve evaluation [27]. We reference this method as "Rs-EL".

Figure 2 shows a comparison of the local series resistance on a Cz-silicon solar cell that was determined with different methods. The images a-c were determined using the same contacting setup for all measurements because the values determined for the local series resistance depend significantly on the contacting details. All measurements in Figure 2 show a good qualitative agreement in the fact that they indicate a circular area of increased local series resistance in the middle right of the cells. A comparison of the two EL-based measurements a and b with an Rs-PL measurement c shows that the local series resistance values determined by the "dark" (=EL) methods tend to be lower than the values determined by the "lighted" method (=PL). A similar behavior is well-known from the determination of the global series resistance. Determining the global Rs from a fit of the dark current voltage curve results in lower series resistance values than that obtained from methods involving illumination. [25] The reason is found in the different current paths between the dark solar cell under current injection and the illumi-

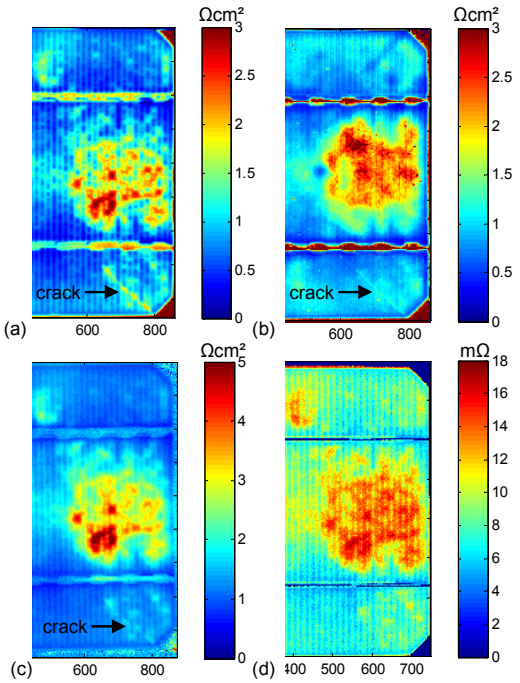


*Figure 2: Comparison of different luminescence imaging methods for the determination of local series resistances on a Cz-silicon cell: (a) Rs-EL, (b) RESI, (c) Rs-PL, (d) CELLO. At the time of the CELLO measurement, there was no crack in the cell. (Measurements a-c by Fraunhofer ISE, d by University of Kiel)*

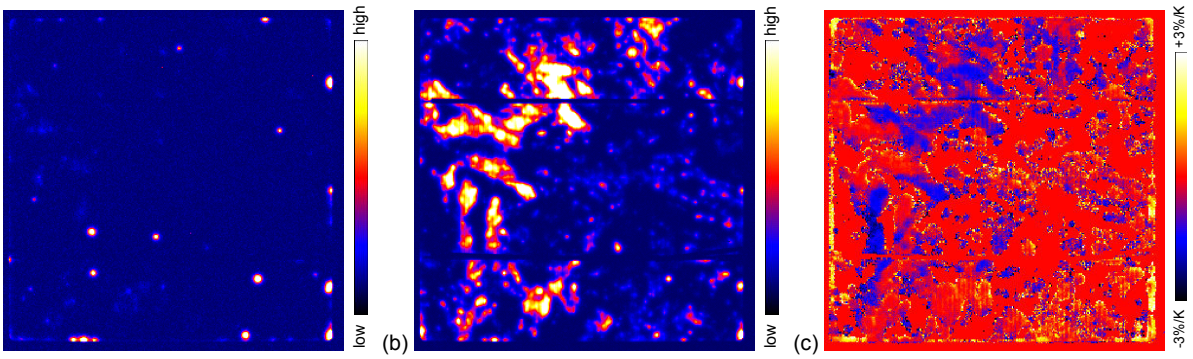


*Figure 3: Dark lock-in thermography images of a multicrystalline silicon solar cell under (a) -7V reverse bias, (b) -14V reverse bias, and (c) temperature coefficient DLIT image at -14V displaying the local temperature dependence of the breakdown current in units of %/K. The scale of the images a and b is proportional to the locally dissipated power. (Measurements by MPI Halle)*

nated solar cell under current extraction. [28]

Future challenges for the determination of local series resistances are firstly, the relation between local series resistances and the (fill-factor-relevant) global series resistance of the solar cell and secondly, the applicability on industrially relevant multicrystalline solar cells. Assumptions currently used by the different methods are well-justified for mono-crystalline cells but their validity for multicrystalline solar cells remains to be tested. Regarding the relation between the local series resistance and the global series resistance, we also included a CELLO [29] measurement in Figure 2d. While the qualitative appearance is similar, the scales and units differ. This is because CELLO uses a different current transport model than the imaging methods described before. The advantage of the current transport model used by CELLO is that the average over all pixels in the series resistance map is directly related to the global series resistance. [29] A further comparison of the different series resistance methods will thus result in a better understanding of the nature of local series resistances and an improvement of the measurement methods.

## IMAGING JUNCTION PRE-BREAKDOWN

The theoretical junction breakdown voltage of an industrial silicon solar cell, with typical base doping densities around $10^{16}$ $cm^{-3}$, should be around -50V. [18] Figure 3, however, shows that the junction already starts to break down at much lower reverse voltages at localized sites. This phenomenon is further referenced as “pre-breakdown”. Figure 3a and b show DLIT measurements of an industrial multicrystalline silicon solar cell under reverse bias. The image scale is proportional to the locally dissipated power. Figure 3a shows several localized points of high power dissipation already at voltages as low as -7V, which are interpreted as points of very early junction breakdown. At a reverse voltage of -14V, great areas of the cell exhibit junction breakdown. Several interesting questions arise with the observation of local pre-breakdown: Which mechanisms cause local pre-breakdown? Does junction breakdown have something to do with material defects? Does pre-breakdown reveal information about material defects?

There are three possible mechanisms for junction breakdown, namely thermal breakdown, Zener breakdown, and avalanche breakdown. [30] Thermal breakdown occurs if the junction temperature becomes so high that silicon becomes intrinsically conductive. For Zener breakdown, the band configuration at the junction must allow for tunneling processes from the conduction band in the n-doped region into the valence band in the p-doped region. This process requires (locally) narrow p-n-junctions, while in wider p-n-junctions, the effect of avalanche breakdown is more likely. In the latter case, a statistically generated electron is accelerated from the p-side to the n-side of the junction by the electric field in the junction. If the electric field increases above a certain threshold value, the kinetic energy of the accelerated electron is sufficient to generate an electron-hole-pair by impact ionization within the junction. These additional free carriers now contribute to the current and can in turn generate other carrier pairs by impact ionization. This avalanche process causes the junction to become conductive in reverse bias. The breakdown current in avalanche breakdown typically decreases with increasing temperature because the maximum kinetic energy achievable by an electron in the junction is limited by collisions with the crystal lattice which are more likely towards higher crystal temperatures due to the increased thermal movement of lattice atoms. The opposite temperature-dependence is observed for Zener breakdown.

To investigate the physical mechanisms behind local junction pre-breakdown on multicrystalline silicon solar cells in more detail, several new DLIT techniques have recently been proposed by some of the authors. [18] The techniques comprise a method for the determination of the local temperature coefficient of the breakdown current

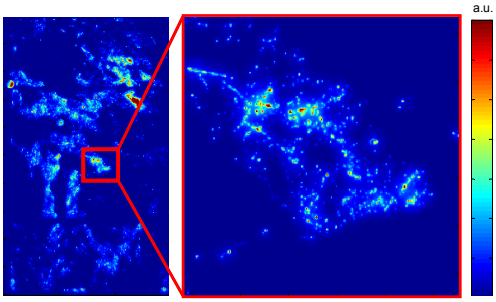


*Figure 4: Light emission from junction pre-breakdown sites at -14V reverse bias on a neighbor cell of Figure 3. The images were captured with a silicon CCD camera. The inset shows that the pre-breakdown "regions" observed in Figure 3 are made up of hundreds of small light spots. (Measurements by Fraunhofer ISE)*

(TC-DLIT), a method to determine the local current multiplication factor in avalanche breakdown (MF-ILIT), and a method to determine the "hardness" of the breakdown (Slope-DLIT). Of these methods, only an example of a TC-DLIT measurement is shown in Figure 3c in this paper while further results can be found in reference [18]. The measurement in Figure 3c shows that the majority of the breakdown regions in this cell exhibits a negative temperature coefficient of the current which indicates break down via the avalanche mechanism.

A phenomenon associated with avalanche breakdown is the appearance of very localized spots of light emission in the visible spectral range [24,31-33]. Values for typical spot sizes are given between 50 and 300 nm in diameter. [30] Some authors attribute this radiation to microdischarge phenomena in so-called miscroplasmas. While the thermo-camera used for the LIT measurements in Figure 3 measures the heat caused by local junction breakdown, a silicon CCD camera can capture the visible light emission directly with a very high resolution, as shown in Figure 4. The resolution of lock-in thermography is limited due to lateral heat spreading in the cell to some value in the range of 1x1 mm² depending on the lock-in frequency [34]. The regions of light emission shown in Figure 4 correlate with the regions of increased heat dissipation in the left half of Figure 3b.

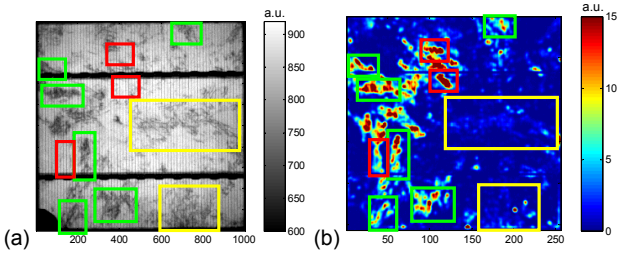


*Figure 5: (a) EL image of a solar cell taken at 0.54V forward bias. (b) DLIT image taken at -14V reverse bias. (Measurements by Fraunhofer ISE)*

Other infrared imaging methods can help to investigate the relation between pre-breakdown and defects in more detail. A number of different observations reported in the literature indicate that there might be a correlation between (light-emitting) breakdown sites and crystal defects like stacking faults and dislocations [31,35,36]. Figure 5 illustrates an interesting relation between defect regions and local junction pre-breakdown. Figure 5a shows an EL image of a multicrystalline cell taken at 0.52V forward bias. The image shows weak and smooth intensity variations caused by variations in the local junction voltage. But more importantly, it shows sharp dendritic regions of strongly decreased intensity which is caused by an extremely low local carrier density due to high recombination at defects. Figure 5b shows a DLIT image of the cell under -14V reverse bias that shows pre-breakdown regions. By comparing the two images we find that many regions of high defect density show up also as pre-breakdown sites (marked in green). There are, however, some pre-breakdown sites that can not be related to defects in Figure 5a (marked in red). A more detailed reverse-voltage dependent analysis indicates that defect-correlated pre-breakdown sites tend to break down at lower reverse voltages than the sites not correlating with high defect densities. There are also regions of high defect density that show up only faintly in the breakdown im-

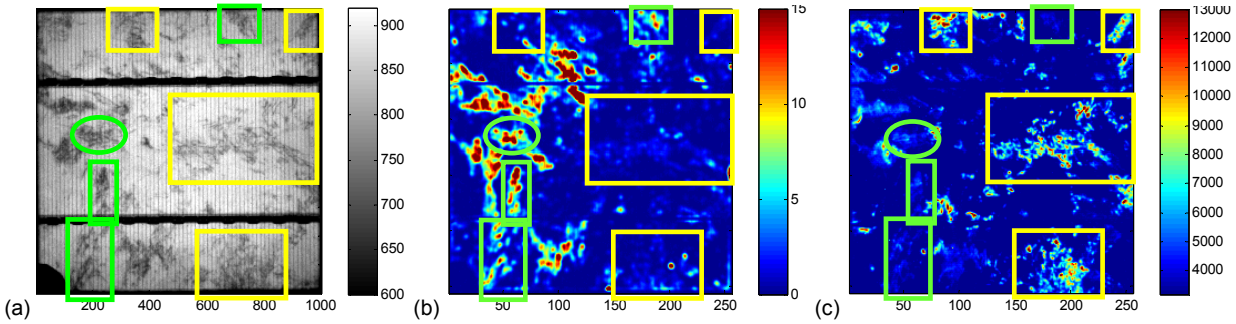


*Figure 6: (a) EL image of a solar cell taken at 0.54V forward bias. (b) DLIT image taken at -14V reverse bias. (c) EL image taken 0.6V with a 1555 nm band-pass filter showing the distribution of sites emitting at the "D1 dislocation line". (Measurements by Fraunhofer ISE)*

age in Figure 5b (marked in yellow).

To take the investigations a step further, we took EL images with an InGaAs camera and a sharp band-pass filter at 1555nm. There are a number of publications indicating that radiation emitted in this wavelength range is emitted by radiative recombination via defect states in the band-gap caused by dislocations. Several authors report emission at different discrete spectral lines for low temperatures and as a broader peak with maximum intensity around 1555 nm at room temperature (often referred to as "D1" line). [7,20,22] Our results in Figure 6 show an interesting and surprising correlation of the "D1" emission with the defect density and the distribution of pre-breakdown regions. Regions of increased defect density (that means reduced intensity in Figure 6a) that show pre-breakdown (Figure 6b) tend to show very low "D1 dislocation line" emission (Figure 6c marked in green). Defect regions that show weak pre-breakdown behavior tend to show strong "D1" emission (marked in yellow).

Further investigations on these effects, using the infrared imaging methods presented in this paper, will shed more light on the pre-breakdown behavior of multicrystalline silicon solar cells in the future.

## ULTRA-FAST INLINE HOT SPOT DETECTION

Module operating conditions can likely occur, where a solar cell is operated at reverse voltages near –10V. Under these conditions, local heating in "hot spots" caused by local pre-breakdown or shunts can easily lead to peak temperatures of several hundred degree centigrade that can damage the cell and the module. Often, the hot spot behavior of a solar cell is deduced from the global values of the shunt resistance or the global reverse current at -10V. This global information, however, is of limited use because for hot spots, the local current *density* or local power *density* is much more important than the corresponding global values. Spatially resolved information is thus especially helpful in this case.

To detect hot spots in an industrial production line we thus propose an ultra-fast DLIT measurement that measures the locally dissipated power. With the locally dissipated power, a reliable and meaningful quantitative measure for hot spot appearance can be obtained in measurement times of only 10 milliseconds.

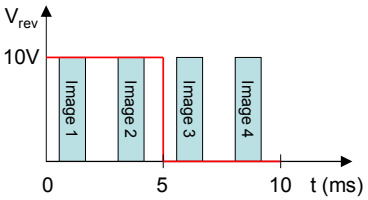


*Figure 7: Timing diagram of a 10 ms DLIT measurement for hot spot detection. The red line indicates the cell reverse voltage and the blue boxes represent the frame integration timing (time for acquisition of a single image from the thermography camera).*

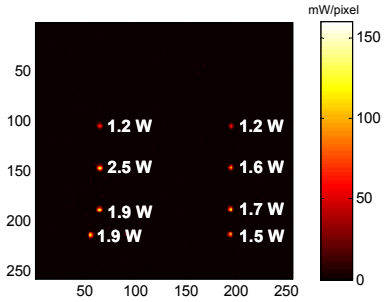


*Figure 8: 10 millisecond hot spot DLIT measurement on an intentionally shunted silicon solar cell at -10 V reverse bias. (Measurement by Fraunhofer ISE)*

Although the term dark lock-in thermography may sound a bit complicated, the method is indeed very simple. The timing diagram in Figure 7 shows the important points in the measurement procedure for the example of a 10 ms measurement. The solar cell is reverse-biased for a period of 5 ms and released to zero Volt for another period of 5 ms. During that time four images are taken by the thermography camera with the image capturing correctly timed in the manner indicated in Figure 7. If $S_i$ with i=1…4 are the frames obtained from the camera, the resulting power-calibrated lock-in image S is then calculated pixel by pixel according to

$$S = \frac{S_2 + S_3 - S_1 - S_4}{\sum_{\forall\ pixels}\left(S_2 + S_3 - S_1 - S_4\right)} \times V \times I \qquad (1)$$

where *V* is the voltage applied to the cell and *I* is the measured global current.[34,37] This calculation procedure can be performed within another millisecond. The resulting power dissipation image can be compared to a preset threshold value and a subsequent automated decision for further processing can be made. Recent experiments indicate for example that shunts can be effectively isolated from the rest of the cell by laser scribing. [38] Whether this process can also effectively eliminate hot spots will be tested in the future.

Figure 8 shows a DLIT image of an intentionally shunted solar cell taken in 10 milliseconds at -10V reverse bias according to the procedure described before. The measurements show that local power dissipation values of 1.2W can easily be determined quantitatively in 10 ms. Measurements of the same cell at lower reverse biases (not shown) indicate that the hot spots can be detected with our setup in 10 milliseconds as soon as the local power dissipation exceeds approximately 0.1W.

## CONLUSIONS AND OUTLOOK

We presented a comprehensive overview over infrared imaging techniques for (electrical) silicon solar cell characterization. Recent method development, especially in local series resistance imaging, was reviewed in detail. We reported a great amount of new and important observations on local junction breakdown in industrial multicrystalline (mc) silicon solar cells and demonstrated an ultrafast method for hot spot detection.

The reviewed methods for local series resistance determination produce a very valuable quantitative information about where problematic series resistance regions are found on the cell. This knowledge is of great help in finding possible causes for an increased global series resistance that is often observed during in-line measurement of current-voltage curves of industrial silicon solar cells.

Local junction breakdown was observed on industrial mc-cells at reverse voltages as low as -7V and breakdown in great areas of the cell at voltages around -14V. As an extension to the experimental results presented in this paper, future research will concentrate on the detailed understanding of the mechanisms behind pre-breakdown and their relation to local material/junction properties. By detecting the “D1 line” emission in this context, we also demonstrated that infrared imaging methods can capture recombination emission from defect states in the band gap in mc silicon solar cells.

Finally, we proposed an ultra-fast, simple and quantitative method for hot-spot detection and demonstrated measurements times in the order of 10 milliseconds for industrially relevant hot spots. With this method, hot spots caused by shunts and local junction breakdown can be reliably detected in a solar cell production line.

## ACKNOWLEDGEMENTS

This work was partially supported by the German Federal Ministry of Education and Research under contract no. 01SF0401 (NETZ DIAGNOSTIK) and by the German Ministry for the Environment, Nature Conservation and Nuclear Safety under contracts no. 0327650D (SolarFocus) and no. 0327616 (PVQC). The authors of the University of New South Wales acknowledge support under the Australian Research Council’s Centres of Excellence Scheme.

## REFERENCES

[1] J. Isenberg, S. Riepe, S.W. Glunz and W. Warta, Journal of Applied Physics 93 (2003) 4268.
[2] M. Bail, J. Kentsch, R. Brendel and M.A. Schulz, Photovoltaic Specialists Conference, 2000. Conference Record of the Twenty-Eighth IEEE(2000) 99.
[3] T. Trupke, R.A. Bardos, M.C. Schubert and W. Warta, Appl. Phys. Lett. 89 (2006) 044107.
[4] P. Würfel, T. Trupke, T. Puzzer, E. Schaffer, W. Warta and S.W. Glunz, Journal of Applied Physics 101 (2007) 123110.
[5] J. Isenberg and W. Warta, Journal of Applied Physics 95 (2004) 5200.
[6] D. Macdonald, J. Tan and T. Trupke, Journal of Applied Physics 103 (2008) 073710.
[7] V. Kveder, M. Badylevich, E. Steinman, A. Izotov, M. Seibt and W. Schroter, Applied Physics Letters 84 (2004) 2106.
[8] M.C. Schubert, S. Riepe, S. Bermejo and W. Warta, Journal of Applied Physics 99 (2006) 114908.
[9] P. Pohl, J. Schmidt, K. Bothe and R. Brendel, Applied Physics Letters 87 (2005) 142104.
[10] J. Isenberg, D. Biro and W. Warta, Progress in Photovoltaics: Research and Applications 12 (2004) 539.
[11] T. Trupke, E. Pink, R.A. Bardos and M.D. Abbott, Applied Physics Letters 90 (2007) 093506.
[12] D. Hinken, K. Ramspeck, K. Bothe, B. Fischer and R. Brendel, International PVSEC-17, Fukuoka, Japan (2007) 5O.
[13] K. Ramspeck, K. Bothe, D. Hinken, B. Fischer, J. Schmidt and R. Brendel, Applied Physics Letters 90 (2007) 153502.
[14] J. Isenberg, A.S.H.v.d. Heide and W. Warta, Prog. Photovolt: Res. Appl. 13 (2005) 697–703.
[15] O. Breitenstein, J.P. Rakotoniaina, A.S.H.v.d. Heide and J. Carstensen, Prog. Photovolt: Res. Appl. 13 (2005) 645–660.
[16] O. Breitenstein, J.P. Rakotoniaina and M.H.A. Rifai, Progress in Photovoltaics: Research and Applications 11 (2003) 515.
[17] M. Kasemann, D. Grote, B. Walter, T. Trupke, Y. Augarten, R.A. Bardos, E. Pink, M.D. Abbott and W. Warta, Progress in Photovoltaics: Research and Applications (2008) (accepted).
[18] O. Breitenstein, J. Bauer, J.-M. Wagner and A. Lotnyk, Progress in Photovoltaics: Research and Applications (2008) submitted.
[19] K. Ramspeck, K. Bothe, J. Schmidt and R. Brendel, Journal of Materials Science: Materials in Electronics DOI: 10.1007/s10854-008-9671-8 (2008).
[20] N.A. Drozdov, A.A. Patrin and V.D. Tkachev, JETP Letters 23 (1976) 597.
[21] M. Kittler, T. Arguirov, A. Fischer and W. Seifert, Optical Materials 27 (2005) 967.
[22] M. Kittler, M. Reiche, T. Arguirov, W. Seifert and X. Yu, physica status solidi (a) 203 (2006) 802.
[23] N. Akil, S.E. Kerns, D.V. Kerns, A. Hoffmann and J.P. Charles, Applied Physics Letters 73 (1998) 871.
[24] N. Akil, S.E. Kerns, D.V. Kerns, A. Hoffmann and J.P. Charles, Electron Devices, IEEE Transactions on 46 (1999) 1022.
[25] D. Pysch, A. Mette and S.W. Glunz, Solar Energy Materials and Solar Cells 91 (2007) 1698.
[26] D. Hinken, K. Ramspeck, K. Bothe, B. Fischer and R. Brendel, Applied Physics Letters 91 (2007) 182104.
[27] J.H. Werner, Applied Physics A: Materials Science & Processing 47 (1988) 291.
[28] A.G. Aberle, S.R. Wenham and M.A. Green, Conference Record of the Twenty Third IEEE Photovoltaic Specialists Conference, 1993 (1993) 133.
[29] J. Carstensen, A. Schütt and H. Föll, Proceedings of the 22nd European Photovoltaic Solar Energy Conference, Milan (2007).
[30] S. Mahadevan, S.M. Hardas and G. Suryan, Physica Status Solidi (a) 8 (1971) 335.
[31] R. Lal and R. Sharan, Solid-State Electronics 29 (1986) 1015.
[32] A.G. Chynoweth and K.G. McKay, Physical Review 102 (1956) 369.
[33] J.W. Bishop, Solar Cells 26 (1989) 335.
[34] O. Breitenstein and M. Langenkamp, Lock-in Thermography - Basics and Use for Functional Diagnostics of Electronic Components, Springer Verlag, Berlin/Heidelberg, 2003.
[35] A.G. Chynoweth and G.L. Pearson, Journal of Applied Physics 29 (1958) 1103.
[36] R.L. Batdorf, A.G. Chynoweth, G.C. Dacey and P.W. Foy, Journal of Applied Physics 31 (1960) 1153.
[37] M. Kasemann, B. Walter, C. Meinhardt, J. Ebser, W. Kwapil and W. Warta, Journal of Applied Physics (2008) (accepted).
[38] Y. Augarten, M.D. Abbott, T. Trupke, R.A. Bardos, H.P. Hartmann, R. Gupta, J. Bauer and O. Breitenstein, Proceedings of the 22nd European Photovoltaic Solar Energy Conference, Milan, Italy (2007) in print.